EuCARD-2

Enhanced European Coordination for Accelerator Research & Development

Note

Mechanical Effects of the Non-Uniform Current Distribution on HTS Coils for Accelerators Wound with REBCO Roebel Cable

Murtomaeki, Jaako (CERN, Geneva, CH and TUT, Tampere, FI) *et al*

30 January 2017

The EuCARD-2 Enhanced European Coordination for Accelerator Research & Development project is co-funded by the partners and the European Commission under Capacities 7th Framework Programme, Grant Agreement 312453.

This work is part of EuCARD-2 Work Package **10: Future Magnets (MAG)**.

The electronic version of this EuCARD-2 Publication is available via the EuCARD-2 web site <http://eucard2.web.cern.ch/> or on the CERN Document Server at the following URL: <http://cds.cern.ch/search?p=CERN-ACC-NOTE-2017-0045>

Mechanical Effects of the Non-Uniform Current Distribution on HTS Coils for Accelerators Wound with REBCO Roebel Cable

J. S. Murtomäki, J. van Nugteren, G. Kirby, L. Rossi, IEEE fellow, J. Ruuskanen and A. Stenvall

***Abstract*—Future high-energy accelerators will need very high magnetic fields in the range of 20 T. The EuCARD-2 WP10 Future Magnets collaboration is aiming at testing HTS-based Roebel cables in an accelerator magnet. The demonstrator should produce around 17 T, when inserted into the 100 mm aperture of Feather-M2 13 T outsert magnet. HTS Roebel cables are assembled from meander shaped REBCO coated conductor tapes. In comparison with fair level of uniformity of current distribution in cables made out of round Nb-Ti or Nb_3Sn strands, current distribution within the coils wound from Roebel cables is highly non-homogeneous. It results in non-uniform electromagnetic force distribution over the cable that could damage the very thin REBCO superconducting layer. This paper focuses on the numerical models to describe the effect of the non-homogenous current distribution on stress distribution in the demonstrator magnet designed for the EuCARD-2 project. Preliminary results indicate that the impregnation bonding between the cable glass fiber insulation and layer-to-layer insulation plays a significant role in the pressure distribution at the cable edges. The stress levels are safe for Roebel cables. Assuming fully bonded connection at the interface, the stresses around the edges are reduced by a large factor.**

***Index Terms*—Superconducting Magnets, Accelerator dipoles, HTS magnets, Mechanical engineering**

I. Introduction

THIS paper presents a new type of modelling of the HTS magnets utilizing Finite Element Analysis (FEA) and presents the relevant steps in the modelling process of impregnated coils wound with Roebel cable for accelerator magnets of the program EuCARD-2 ([1], [2], [3], [4], [5]).
Usually, the coils of the LTS magnets have been modelled as block domain coil pack utilizing anisotropic material properties for the central cross-section of the coil [6], [7]. The HTS impregnated coil (Fig. 1) requires a new approach, since the correct mechanical behavior is difficult to reproduce due to partially non-impregnated structure of the coil playing an important role in the stress distribution. Due to low pressure between turns during the impregnation, the epoxy does not enter between the strands (tapes), leaving them non-bonded. The tape geometries can be seen in Fig. 1, Fig. 2, Fig. 3. More details about impregnation can be found in [8]. Frictional contacts between the tapes are shown in Fig. 4. Various tapes forming the cable can slide with respect to each other on the wide planar strand-to-strand interface.
The foreseen computed non-uniformity of the current distribution on the planar conductor surface of the strand requires additional modeling details (see Fig. 5). The model needs a separate conductor geometry to correctly locate the forces on the planar conductor surface of the strands. It is not possible to ignore this detail because the primary aim of this paper is to compute the compression distribution perpendicular to the wide face of the conductor. A further goal of this model is to compute the stress distribution in the strands and the insulation due to cool down and evaluate the shear stress level between the surface of the strand and impregnated insulation interface. In addition, the model is used to study the conductor sensibility to interfacial delamination due to differential thermal contraction of the insulation and the strand materials, which is one of the issue considered critical for the use of REBCO tape in impregnated magnets. ANSYS Workbench® environment is used for this modelling task.

Manuscript received January 30, 2017. This work was supported in part by EuCARD-2. EuCARD-2 is co-funded by the partners and the European Commission under Capacities 7th Framework Programme, Grant Agreement 312453. Authors J. Murtomäki is with Dept. of Electrical Engineering, Tampere University of Technology (TUT), Tampere, Finland and with CERN, TE/MSC/MDT, Geneva, Switzerland, J. van Nugteren is with The University of Twente, Twente, Netherlands and with CERN, TE/MSC/MDT, Geneva, Switzerland, G. Kirby and L. Rossi are with CERN, Accelerator & Technology Sector, Geneva, Switzerland, A. Ruuskanen and A. Stenvall are with Dept. of Electrical Engineering, Tampere University of Technology (TUT), Tampere, Finland

II. Modelling discussion

A. General

This work consists of modelling the Feather-M2 aligned block coil, the main deliverable of EuCARD-2-WP10 program (see [2]). The coil is an $800\,\mathrm{mm}$ long race track dipole, where each pole is composed of a two-layer coil (see Fig. 1). A detailed 2D FEA [9] model with plane strain assumption is taken as a modelling basis. This approach is a good 2D approximation for infinitely long continuous structures in the 3rd dimension [10]. The model is assumed to be symmetric over y- and x-axis for convenience, even if in reality the magnet is not fully symmetric. The magnet has a peculiar support structure compared to usual dipole magnets. The main author's work in progress FEA indicates the need to connect outer and inner shell by a stiff plate in the mid-plane due to requirement to prevent shell from touching the outsert magnet during powering at the rightmost point of the outer shell on the mid-plane (Fig. 1, see also details in [11]).

B. Strand level

The strand (tape) structure is simplified to a Hastelloy or a stainless steel substrate domain, and an electroplated copper

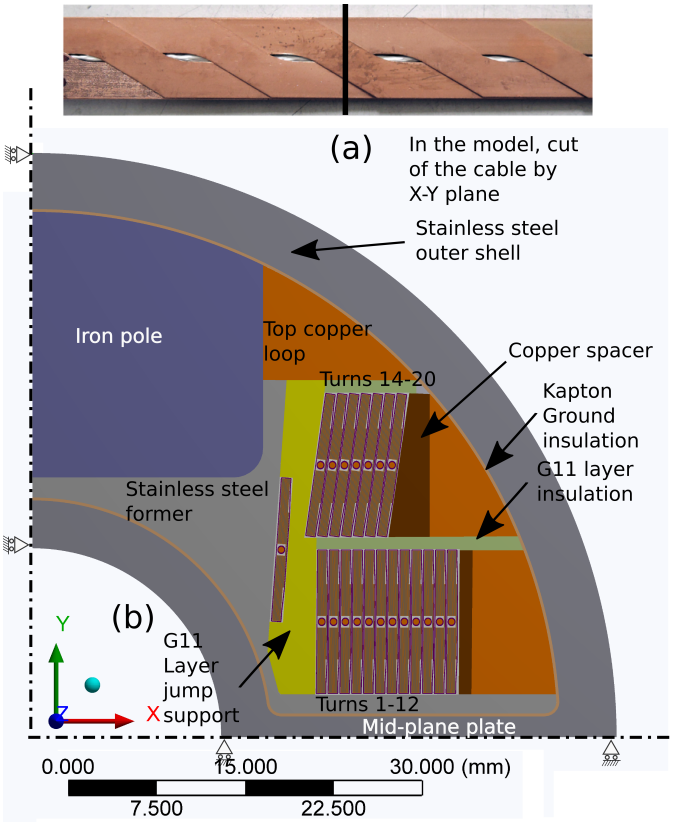

Fig. 1. (a) Non-impregnated Roebel cable view without a glass-fiber sleeve. It is viewed from the wide face direction of tapes showing the location of the cut of the cable model. The tapes are in frictional contact after impregnation, as the epoxy does not enter between them. [8] (b) Feather-M2 magnet model central cross-section. Warp direction of Layer jump support corresponds to y-axis and warp direction on G-11 layer insulations correspond to x-axis. The narrow dimension in both corresponds to thickness direction of the fibers.

jacket domain (coating domain) surrounding the substrate (Fig. 2-Fig. 4). Actually, the copper jacket does not have uniform thickness and perfect rectangular shape due to imperfect electroplating, however these imperfections (in particular the so-called dog-bone shape of the copper jacket) are neglected in the model. It is thus possible to have a regular mesh on the straight contact surfaces with nodes located on the same point on each side of the tape-to-tape contact. The contacts can therefore reduce the nonlinear computational effort, and it is also possible to reduce the number of elements. This approach results in total of 280 contact surface pairs between the tapes. The pressure distribution of Fig. 5 can be imported on the nodes on the line that is between the substrate domain and the coating domain (Fig. 3). These two domains share nodes on their interface, which implies coupling of all degrees of freedom in each node. For the turn #1 next to the layer jump (Fig. 1), the volume of the glass-resin composite next to the conductor can be locally relatively large. It is therefore important to investigate the possible conductor layer shear stress at that location during the cool down. The wide face of the coating can be modelled with nodes on both domains and then connected with Multi Point Constraint (MPC) [12] bonded contact approach.

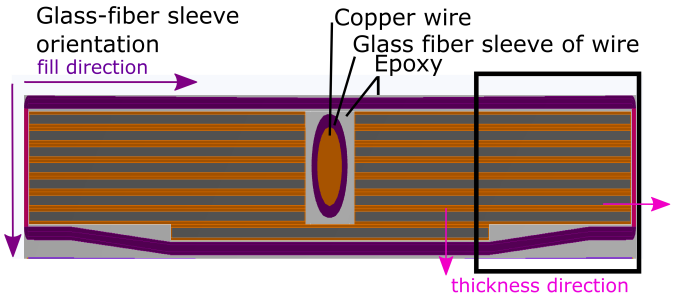

Fig. 2. A 15 strand Roebel cable cross-section. The picture has been magnified vertically for detail view. REBCO tape substrate is in dark grey, copper in orange, glass sleeve in dark violet and resin rich zone in light grey. The warp direction of the GF Sleeve is along the cable axis.

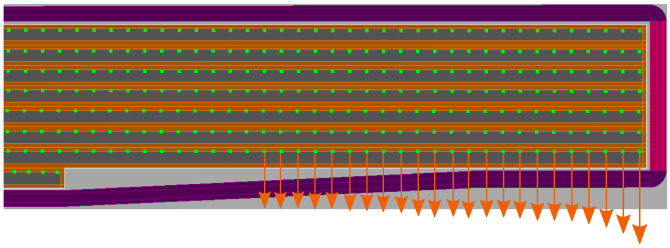

Fig. 3. A magnification of the right zone of Fig. 2. Pressure import on conductor is represented by the arrows on green nodes, shared by the Cu- and substrate material domains.

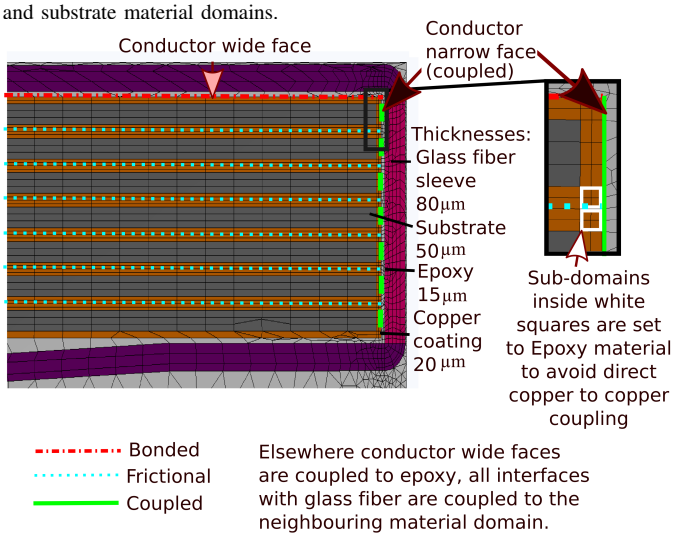

Fig. 4. Cable dimensions and connections. The full cable domain is 12.3 x 1.13 mm, the conductors are 5.5 mm wide.

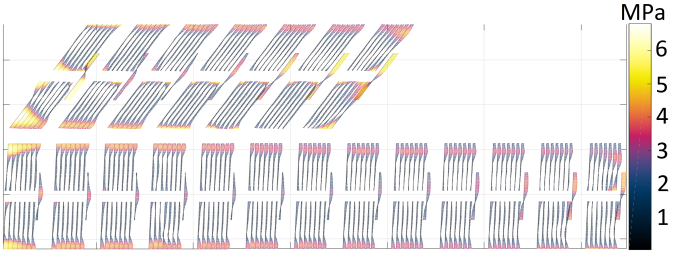

Fig. 5. The imported horizontal pressure distribution on the individual tapes resulting from the non-uniform current distribution (see [4]). The superconductor and buffer layers are not explicitly modelled, Radial dimension of the coil is magnified by factor 6 compared to real dimensions.

TABLE I
THERMAL CONTRACTION FROM 293 K TO 4 K

Material	G-11	G-11	G-11	CTD-101K	Kapton
Dimens.	thickness	warp	fill	isotr.	isotr.
10^{-3}	6.20	2.10	2.10	12.08	4.4
Ref.	[13]	[13]	[13]	[14]	[15]
Material	GF Sleeve	GF Sleeve	GF Sleeve	OFCH Cu	SS304
Dimens.	thickness	warp	fill	isotr.	isotr.
$10^{-}3$	5.95	1.95	1.95	3.23	2.97
Ref.	[16]*	[16]*	[16]*	[14]	[17]

TABLE II
E-MODULUS [MPA]

Material	G-11	G-11	G-11	CTD-101K	Kapton
Dimens.	thickness	warp	fill	isotr.	isotr.
4 K	22000	39400	32900	(6440)	2500
76 K	(18650)	37300	31100	(6420)	2500
295 K	(14406)	32000	25500	4400	2500
Ref.	[18]*	[19]	[16]*	[20]*	[21]
Material	GF Sleeve	GF Sleeve	GF Sleeve	OFCH Cu	SS304
Dimens.	thickness	warp	fill	isotr.	isotr.
4 K	19700	39400	32900	117000	210000
76 K	16700	37300	31100	117000	215000
295 K	12900	32000	25500	117000	199500
Ref.	[16]*	[19]	[16]*	[22]	[17]

TABLE III
POISSON'S RATIO

Material	G-11	G-11	G-11	CTD-101K	Kapton
Dimens.	th-warp	warp-fill	th-warp	isotr.	isotr.
4 K	(0.12)	0.212	0.22	0.30	0.34
76 K	(0.13)	0.22	0.21	0.30	0.34
295 K	0.09	0.16	0.15	0.30	0.34
Ref.	[23]*	[19]	[19]	[24]*	[21]
Material	GF Sleeve	GF Sleeve	GF Sleeve	OFCH Cu	SS304
Dimens.	th-warp	warp-fill	th-warp	isotr.	isotr.
4 K	(0.12)	0.21	0.22	0.34	0.30
76 K	(0.13)	0.22	0.21	0.34	0.30
295 K	0.09	0.16	0.15	0.34	0.30
Ref.	[23]*	[19]	[19]	[25]*	[25]*

TABLE IV
SHEAR MODULUS [MPA]

Material	G-11	G-11	G-11	CTD-101K	Kapton
Dimens.	th-warp	warp-fill	th-warp	isotr.	isotr.
4 K	(4917)	9000	9000	2403	933
76 K	(4169)	(7629)	(7629)	2396	933
295 K	3220	(5893)	(5893)	1642	933
Ref.	[23]*	[18]*	[18]*	**	**
Material	GF Sleeve	GF Sleeve	GF Sleeve	OFCH Cu	SS304
Dimens.	th-warp	warp-fill	th-warp	isotr.	isotr.
4 K	(4917)	9000	9000	43657	80769
76 K	(4169)	(7629)	(7629)	43657	82692
295 K	3220	(5893)	(5893)	43657	76731
Ref.	[23]*	[18]*	[18]*	**	**

Due to lack of material property data, some material properties are replaced by similar materials. These references are marked by *. Some values are in brackets to indicate that the value has been extrapolated. For the shear modulus of isotropic materials, marking by ** at the reference column means that the values are computed using Poisson's ratio and E-modulus. In this analysis SS304 represents all stainless steel structures and substrate domains in the computation. The GF sleeve is S-2 493 33 [26] impregnated with CTD-101K.

C. Cable level

With respect to the actual 3D cable geometry, in the 2D model an ideal position of each tape is assumed, i.e. without longitudinal slippage of tapes due to winding effect. The cable model includes a domain for the central filler wire, see Fig. 2. It was introduced to reduce resin volume, limiting stress concentration due to thermal contraction, and for constraining the movement of the tapes towards the cable central gap. [27] Frictional contacts between the tapes inside each cable are assumed. The coefficient of friction (CF) is iteratively increased to test the sensitivity of the sliding with respect to the CF. It is assumed that the tapes do not slide very easily, and a CF=0.2 is chosen at the limit of tapes not moving due to part of the e.m. forces acting parallel to the strand surface. With a higher CF value, shear stresses between the tapes are higher, which implies that the coil experiences less deformation in the vertical direction. We believe that CF=0.2 is a conservative value, but this point needs to be more deeply investigated.
Cable insulation, i.e. impregnated glass fiber (GF) sleeve with resin impregnation, is modelled as a separate domain (Fig. 2-Fig. 4) composed of four rectangular sub-domains that allow anisotropic material properties along the two axis. All mechanical properties are summarized in the Table I-Table IV. The connection between the insulation and the tape is intricate. The GF and epoxy have very different E-moduli and coefficient of thermal expansion. An intermediate epoxy layer is assumed around the GF domain. Due to this the shear stress build-up due to cool down is reduced and more realistic. Thus the tapes are all assumed to be connected to composite through thin epoxy layer by coupling as shown in Fig. 4. It is assumed that the epoxy does not delaminate on the narrow faces of the tapes due to cool down. An important modelling assumption is taken in order to reduce computational time: the narrow face of the copper jacket shown in the Fig. 4 is coupled with the epoxy domain (that is coupled with the GF domain). In the model, nodes on two different domains, and located at the same point are merged into one single node, thus coupling all degrees of freedom between the domains.

D. Magnet assembly level

Thanks to the use of mould release agent during winding on the former surfaces, the impregnated coil pack can separate from the vertical surfaces. The horizontal surfaces of the former and lower surface of the top copper loop allow horizontal movement of the coil turns towards the stainless steel shell. These surfaces are modelled as frictional contact surfaces, having CF=0.2. During the impregnation, the epoxy resin enters in between the parts of the assembly cross-section, bonding the various surfaces together. However, due to very low E-modulus of the epoxy, we assume that the iron pole, top copper loop and former (Fig. 1) can move easily relative to interfacing domains. The coil pole is impregnated before inserting it into the stainless steel shell, so the surfaces of the former are not coupled to the ground insulation. The copper loops at the coil level may move easily relative to all interfacing parts, except Kapton ground insulation, where it is bonded. Frictional contacts are used in all these above mentioned interfaces. This approach avoids coupling interfaces between materials with high E-modulus, and thus making the assembly unrealistically stiff.

E. Elements and load steps

The material domains of model are based on Plane183 element that includes all the necessary degrees of freedom [28]. The element mid-nodes are turned on. Additional features include non-linearity of the stiffness matrix and temperature dependent material properties (see Table I-Table IV). There is no account taken for plastic deformation in this initial analysis phase. Roughly 600.000 nodes form sufficient mesh. At the thin copper coating domains, there are at minimum two elements for the thickness direction of the coating, but the aspect ratio of the elements is large. However, the almost unidirectional pressure distribution can be computed with this initial mesh geometry.

The first load step is the cool down from room temperature (293 K) to 4.2 K. In the second step, powering at 17 T (attained in insert mode with 13 T background), the non-uniform force distribution in the modelling plane is imported from the electromagnetic model that computes forces in 3D [4]. The downwards pulling force of the iron pole 58 N/mm (mm along z-axis) was computed using ANSOFT Maxwell in 3D and added on the low boundary of the iron to approximate the load on this domain.

III. Results Discussion

In the Fig. 6, the stress field is shown at maximum field (17 T) in the case of simplified model, where the coils can slide against an infinitely rigid radial support. Compression level occuring inside one element thickness at the edge reaches up to 400 MPa (Fig. 6 (a)). Outside the singularities, 220 MPa is maximum. For comparison, a case where forces are averaged over the full coil is shown (Fig. 6 (b)). In the full-scale model (Fig. 1), the cool down generates $10-30$ MPa shear on the epoxy at the surfaces of the tapes. According to [29], this level of shear likely leads to epoxy delamination from the coating

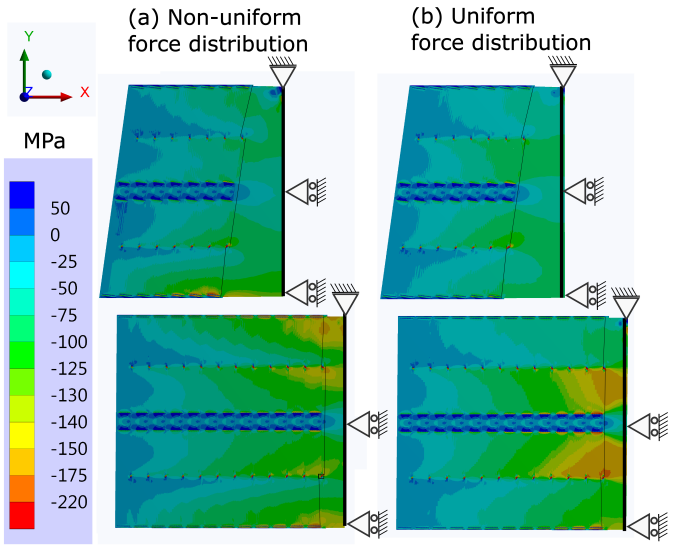

Fig. 6. The case of the coil without external structures to show the natural horizontal pressure distribution of the coil at 17 T field due to (a) non-uniform and (b) uniform force distribution. In the latter, the forces concentrate in the middle of the cable.

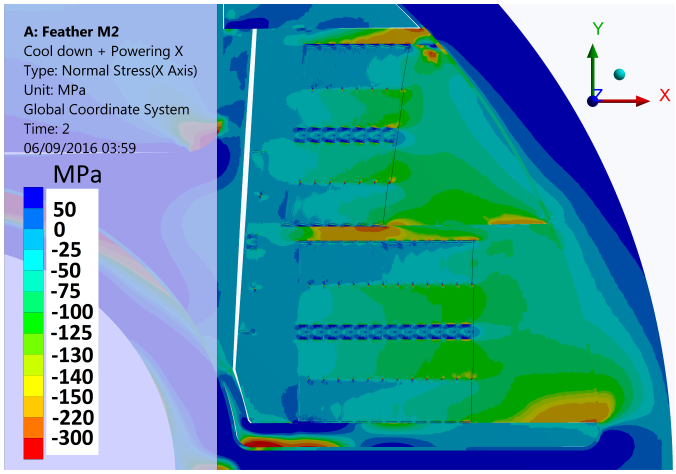

Fig. 7. The horizontal pressure distribution [MPa] in the coil due to non-uniform force distribution after cool down and powering at 17 T.

surface as the maximum shear stress of $8-10$ MPa is exceeded. Due to the likely delamination at low shear level, HTS conductors are protected from fracturing due to cool down. The G-11 layer insulation located in the middle of the coil has smaller thermal contraction in the horizontal direction than the composite coil domains in the same direction. After cool down we can observe 80 MPa shear stress between the cable GF insulation and G-11 layer insulation bonded by the epoxy. Shear strenght of epoxy at 76 K is 85 MPa [16]. However, this model is limited for evaluation of shear stress, as the conductor narrow face is not allowed to delaminate and relieve portion of shear stress. If the full delamination occurs between the coil and layer insulation, the coil stress distribution will resemble more Fig. 6 than Fig. 7. The distribution of the e.m. forces concentrates on the edges of the conductor, and it can be seen that the copper would plastically deform in any case, as the elastic limit (35 MPa [30]) of annealed copper is exceeded in coating and copper loops. If full coupling between the G-11 and the coil insulation is assumed in the powering of the coil, the stress concentrations from the edges of the tapes are supported by the G-11. This lowers the peak stress of the tapes of the most loaded turns to -150 MPa (Fig. 7), and the stress distribution on conductor is more uniform.

IV. Conclusion

The non-uniform stress distribution was computed for the Feather-M2 magnet. Due to impregnation we may experience delamination of the epoxy at the tape surface due to cool down. This is beneficial, since the delamination likely occurs at very low shear stress levels, protecting the HTS conductor. A measurement was recently performed at The University of Twente for a cable under uniform transverse pressure. No degradation of I_C was seen at 450 MPa [31]. If mould release agent is applied on the G-11 layer insulation before impregnation, the layer insulation deliberately delaminates from the coils due to cool down. This makes the coil mechanically more predictable, and is a viable option. According to the computations, even in the case of Fig. 6 the stress level -220 MPa due to the non-uniform current distribution is reasonable.

REFERENCES

[1] L. Rossi *et al.*, "The EuCARD-2 Future Magnets European collaboration for accelerator quality HTS magnets," *IEEE Transactions on Applied Superconductivity*, vol. 25, no. 3, June 2015.

[2] G. Kirby, J. van Nugteren, A. Ballarino *et al.*, "Accelerator Quality HTS Dipole Magnet Demonstrator Designs for the EuCARD-2, 5 T, 40 mm Clear Aperture Magnet," *IEEE Transactions on Applied Superconductivity*, vol. 25, no. 3, June 2015.

[3] J. van Nugteren, G. Kirby, G. de Rijk *et al.*, "Study of a 5 T Research Dipole Insert-Magnet Using an Anisotropic ReBCO Roebel Cable," *IEEE Transactions on Applied Superconductivity*, vol. 25, no. 3, pp. 1–5, June 2015.

[4] J. van Nugteren, "High Temperature Superconductor Accelerator Magnets," Ph.D. dissertation, University of Twente, 2016, the non-homogenous surface force density distribution plot is at page 162. Thesis is available at: https://cds.cern.ch/record/2228249/files/CERN-THESIS-2016-142.pdf.

[5] G. Kirby, L. Rossi, M. Bajko *et al.*, "Status of the Demonstrator Magnets for the EuCARD-2 Future Magnets Project," *IEEE Transactions on Applied Superconductivity*, vol. 26, no. 3, April 2016.

[6] C. Kokkinos and M. Karppinen, "High Gradient Nb_3Sn Quadrupole Demonstrator MKQXF Engineering Design," CERN-ACC-NOTE-2016-0039, 2016.

[7] M. Karppinen, N. Andreev, G. Apollinari *et al.*, "Design of 11 T Twin-Aperture Nb3Sn Dipole Demonstrator Magnet for LHC Upgrades," *IEEE Transactions on Applied Superconductivity*, vol. 22, no. 3, June 2012.

[8] J. van Nugteren, "High Temperature Superconductor Accelerator Magnets," Ph.D. dissertation, University of Twente, 2016, at page 34 it is stated: "The pressure prevented the resin from entering between the tapes.".

[9] M. Turner, R. Clough, H. Martin *et al.*, "Stiffness and deflection analysis of complex structures," *J. Aera. Sci.*, vol. 23, pp. 805–23, 1956.

[10] F. David and H. Nolle, "Experimental Modelling in Engineering," Elsevier, p. 136, 2013.

[11] J. van Nugteren, "High Temperature Superconductor Accelerator Magnets," Ph.D. dissertation, University of Twente, 2016, the statement at page 73-4.

[12] *ANSYS Workbench help 16.2, Multi-Point Constraint (MPC) Contact Formulation*, ANSYS.

[13] J. Ekin, "Experimental Techniques for Low-temperature Measurements: Cryostat Design, Materials Properties, and Superconductor Critical-Current Testing," Oxford University Press, p. 602, 2011.

[14] G. Kirby, V. Datskov, S. Clement, A. Chiuchiolo, P. Fessia, R. Gauthier, G. Lynch, J. Murtomäki, J. van Nugteren, F. Pincot, J. C. Perez, L. Rossi, G. De Rijk, S. Tavares, and V. o. Venturi, "Thermal contraction, Experimental Data and Fits for the Thermal Contraction of Future Magnet Materials at Cryogenic Temperatures," CERN, February 2016.

[15] *Material properties for Polyimide (Kapton)*, National Institute of Standards and technology, Material Measurement Laboratory, Cryogenic Technologies Group, retrieved 3.6.2015, Available at: http://cryogenics.nist.gov.

[16] *CTD-101K Datasheet*, Composite Technology Development, Inc, the properties for our GF sleeve are taken from the data in this document for S-Glass weave, 50 % Vf impregnated with CTD-101K, Retrieved 28.9.2016, Available at: http://ncsx.pppl.gov/.

[17] *Material Properties for 304 Stainless steel (UNS S30400)*, National Institute of Standards and technology, Material Measurement Laboratory, Cryogenic Technologies Group, retrieved 3.6.2015, Available at: http://www.cryogenics.nist.gov.

[18] K. Timmerhaus and R. Reed, "Cryogenic Engineering: Fifty Years of Progress," International Cryogenics Monograph Series, p. 73, 2007, material properties for HPL (G-10CR).

[19] M. Kasen, G. MacDonald, D. Beekman Jr., and R. Schramm, "Mechanical, electrical, and thermal characterization of G-10CR and G11CR glass-cloth/epoxy laminates between room temperature and 4 K," available at: http://ncsx.pppl.gov.

[20] *Material properties for G-11CR resin*, Material Property Database, MPDB v 7.43 software, for G-11CR, the reference given in the program is: H.M. Ledbetter and G. Maerz, Cryogenics, v20, p655 (1980).

[21] *DuPont Kapton HN polyimide film Technical Data Sheet*, DuPont, available at: http://www.dupont.com/content/dam/dupont/products-and-services/membranes-and-films/polyimde-films/documents/DEC-Kapton-HN-datasheet.pdf.

[22] J. Ekin, "Experimental Techniques for Low-temperature Measurements: Cryostat Design, Materials Properties, and Superconductor Critical-Current Testing," Oxford University Press, p. 592, 2011.

[23] D. Samborsky, J. Mandell, and P. Agastra, "3-D Static Elastic Constants and Strength Properties of a Glass/Epoxy Unidirectional Laminate," available at: http://www.montana.edu.

[24] Epotek, "Understanding Mechanical Properties of Epoxies For Modeling, Finite Element Analysis, (FEA)," available at: http://www.epotek.com.

[25] M. Pojer, A. Devred, and W. Scandale, "A Non-Linear Finite Element Model for the LHC Main Dipole Coil Cross-Section," *Presented at the 19th International Conference on Magnet Technology (MT19) Genova, Italy*, September 2005.

[26] AGY, "AGY Product information, 493 S-2 Glass Yarn," available at: http://www.agy.com.

[27] *Continuously transposed conducting cable*, Provisional European patent application No. EP15179513.5., CERN, (inventors J.S Murtomäki, J. van Nugteren and G. Kirby, G.), 2016.

[28] *ANSYS Mechanical APDL Element Reference 15.0*, ANSYS.

[29] X. Deville, "Test Report - Shear test results - Influence of the ceramic binder CTD-1202 and reaction cycle on MQXFS cable epoxy bonded joints, checked by S. Tavares, approved by G. de Rijk, EDMS number 1719997 v.1," CERN, in this report a lap shear test between two MQXFS cables is performed. The cables are made of forty 0.85 mm diameter Nb_3Sn wires, with the glass fibre insulation S-2 fibre, size 933 from AGY impregnated on it. It gives an indication of the level of average maximum shear stress that can be expected for CTD-101K bonded to a copper surface composing of a round strands of Nb_3Sn cable in room temperature. For HTS tapes, it can be taken as an indicative value.

[30] *Material properties for copper*, Material Property Database, MPDB v 7.43 software, for annealed Copper (42 micron GS), the reference given in the program is: N.J. Simon, et al., NIST monograph 177, Properties of Copper and Copper Alloys at Cryogenic Temperatures (1992).

[31] P. Gao *et al.*, "Effect of tape layout and impregnation method on the transverse pressure dependence of the critical current in REBCO Roebel cables," *presented at this conference, ASC2016 paper ID is 2LPo2D-06*, 2016.